ECS Transactions, 25 (1) 3-13 (2009)
10.1149/1.3210554 ©The Electrochemical Society

Model to Investigate Interfacial Morphology Effects on Polymer Electrolyte Fuel Cell Performance

Hemant Bajpai[a], Manish Khandelwal[a,b], E. C. Kumbur[a,c], and M. M. Mench[a,*]

[a] Fuel Cell Dynamics and Diagnostics Laboratory, Department of Mechanical Engineering, The Pennsylvania State University, University Park, PA 16802 USA
[b] Current affiliation: UTC Power, South Windsor, CT 06074 USA

[c] Current affiliation: Department of Mechanical Engineering and Mechanics, Drexel University, Philadelphia, PA 19104 USA
[*] Corresponding Author (mmm124@psu.edu)

The purpose of this work is to investigate the impact of the interfacial contact morphology between the catalyst layer (CL) and micro porous layer (MPL) on the polymer electrolyte fuel cell (PEFC) performance. A single-phase anisotropic mathematical model has been developed to evaluate the role of interfacial morphology on ohmic, thermal and gas-phase transport. The novel feature of the model is inclusion of directly measured surface morphological information of the cathode catalyst and the micro porous layers. The preliminary results indicate that thermal disruption due interface morphology has low absolute impact in comparison to ohmic disruption. Ultimately, this model will be used as a tool to understand and minimize the PEFC performance loss, and to develop guidelines for optimal CL and MPL surfaces.

Introduction

Even though substantial technological improvements have been made over the past decade, several technical barriers must be overcome for successful commercialization of Polymer electrolyte fuel cells (PEFCs). To improve PEFC performance, all losses must be clearly understood and accounted in the cell and stack design. A significant source of losses originates from the contact among various fuel cell components, namely micro porous layer (MPL), catalyst layer (CL), MPL|Macro diffusion media (DM) and DM|bipolar plate (BP). Special attention is required for the MPL|CL interface as it acts as a bridge between the reacting and non-reacting components. Variation in the surface morphology and pore size distribution of CL and MPL may lead to imperfect mating and can form interfacial gaps. This improper mating can increase the contact resistance and affect PEFC performance. Some experimental studies were performed to quantify the various interfacial resistances [1-2]. The study reported by Makharia *et. al.* was devoted to identify the MPL|CL interfacial resistance [3]. In this work, they demonstrated an impedance measurement method for resolving voltage losses due to ohmic resistance in the cell. These interfacial resistances can be further enlarged by severe PEFC operating environment especially during sub-zero environment or load cycling. Experimental and modeling freeze/thaw studies at Penn State FCDDL have already shown existence of these interfacial gaps and its effect on cell resistance [4-7]. Most of these studies focused on increase in ohmic resistance due to the contact. However, these interfacial gaps at the

CL|MPL interface may also act as a potential location for liquid water pooling and can therefore affect the mass transport.

The current study is motivated by the need to obtain a better understanding of the CL|MPL interface on local ohmic, thermal and gas-phase mass transport losses. In the present work, a single-phase anisotropic mathematical model has been developed to investigate the impact of interfacial morphology on PEFC performance. Interfacial morphology information of catalyst layer and the micro porous layer were experimentally characterized and integrated into computational framework as a discrete interface layer.

Model Formulation

This section describes the detailed derivation of the single-phase model. The schematic of the fuel cell and its components, and control volume for the model development is shown in Figure 1. Conservation of mass, energy and charge have been performed for each fuel cell component as described.

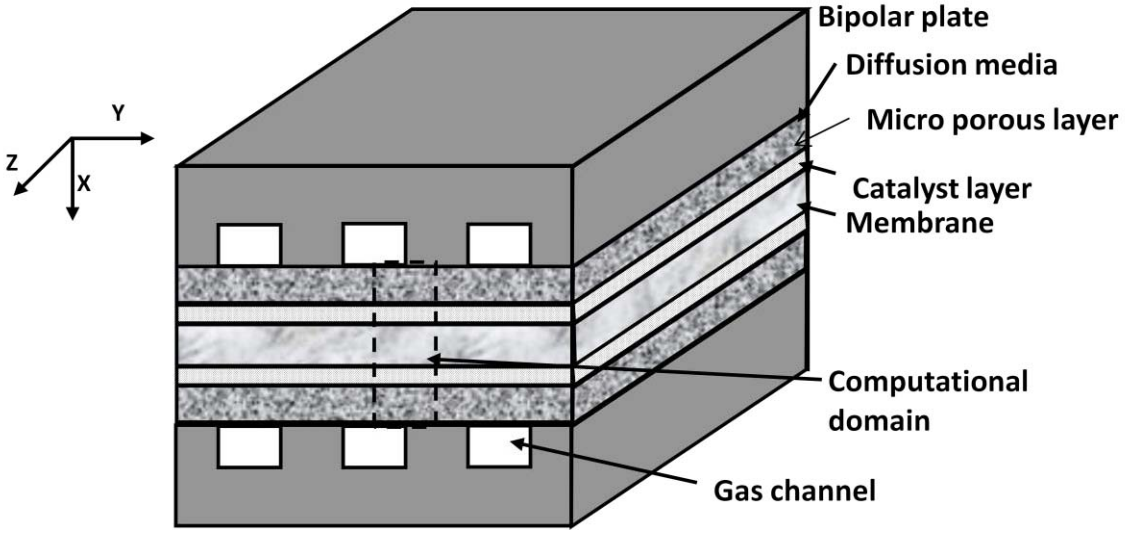

Figure 1. Schematic and control volume for the model formulation

Model Assumptions

The following assumptions were made for the development of the single-phase PEFC model:

1. Model is developed in two-dimension and has reached steady state.
2. MPL, diffusion media (DM) and CL are considered to be porous media. The polymer electrolyte membrane (PEM) is treated with a pure diffusion model.
3. All material properties are homogenous and anisotropic.
4. Conduction is assumed to be the dominant mode of heat transfer in the fuel cell components, whereas convective heat transfer due to flow of reactant gas species is neglected.
5. Joule heating is neglected in the MPL and DM due to relatively high electrical conductivity.

Species Transport

Species transport was derived for the reactant and product gases on the anode and cathode sides. A generalized form of Fick's law was used for the species transport. Species transport was solved for H_2 and H_2O on the anode side and O_2, N_2 and H_2O on the cathode side [8]:

$$D_i^{eff} \frac{\partial^2 C_i}{\partial x^2} + D_i^{eff} \frac{\partial^2 C_i}{\partial y^2} + S_i = 0 \quad [1]$$

where C_i is the molar concentration, D_i^{eff} is effective diffusion coefficient and S_i is the source term for species. The first and second term in the Eq. 1 represent the through-plane (x-direction) diffusion and in-plane diffusion of reactant and product gases. The last term in Eq. 1 represents the consumption/production of the reactant species. This source term is non-zero in the catalyst layer and zero in other components. For H_2 and O_2, the source term in the catalyst layer can be written as:

$$S_i = -\frac{s_k J_{gen}}{nF} \quad [2]$$

where s_k is the stoichiometry coefficient, n is the number of electrons transferred, J_{gen} is the transfer current density and F is Faraday's constant. For water, the source term in the catalyst layer has an additional electro-osmotic drag term and can be written as:

$$S_i = -\frac{s_k J_{gen}}{nF} - \nabla.\left(\frac{n_d}{F} i_e\right) \quad [3]$$

where n_d is electro-osmotic drag coefficient for water and i_e is ionic current. Thermo-osmotic flow in the membrane [9] is not included in the present formulation, but will be considered in the future work. For the porous regions of a PEM fuel cell, diffusivity expression is modified to account for the toruosity effect using Bruggman correlation as:

$$D_i^{eff} = \varepsilon^{1.5} D_i \quad [4]$$

where ε is the porosity of the medium.

Energy Transport

Conduction is the dominant heat transfer mode in the porous fuel cell components [10]. To perform the energy conservation, advection heat transport due to vapor diffusion and reactant/product species is neglected. The generalized energy equation in all the PEFC components can be written as [11]:

$$k_x \frac{\partial^2 T}{\partial x^2} + k_y \frac{\partial^2 T}{\partial y^2} + S_{gen} = 0 \quad [5]$$

where T is the temperature, k_x, k_y is the thermal conductivity in x-y direction (anisotropic properties) and S_{gen} is the source term. The first and second term in the Eq. 5 represents

the through-plane and in-plane thermal transport respectively. In catalyst layer, the source term can be represented as:

$$S_{gen} = J_{gen}\left(\eta + \frac{T\Delta S}{nF}\right) + \frac{{i_e}^2}{\kappa} + \frac{{i_s}^2}{\sigma} \quad [6]$$

where η is overpotential, ΔS is entropy change, i_e is ionic current, i_s is electronic current, κ is ionic conductivity and σ is the electronic conductivity. These four terms represent irreversible heat of the electrochemical reaction, reversible entropic heat and Joule heating because of ionic and electronic current. In the membrane, source term only has Joule heating because of ionic current which can be represented as:

$$S_{gen} = \frac{{i_e}^2}{\kappa} \quad [7]$$

Charge Transport

In the PEFC, protons travel through the ionic conductor (membrane and ionomer in the CL) while electrons transfer through the solid matrix (CL, MPL and DM). Conservation of charge is performed for both proton and electron, and can be written as [8]:

Protons Transport: $$\kappa_x \frac{\partial^2 \varphi_e}{\partial x^2} + \kappa_y \frac{\partial^2 \varphi_e}{\partial y^2} + J_{gen} = 0 \quad [8]$$

Electrons Transport: $$\sigma_x \frac{\partial^2 \varphi_s}{\partial x^2} + \sigma_y \frac{\partial^2 \varphi_s}{\partial y^2} - J_{gen} = 0 \quad [9]$$

where φ_e and φ_s are the membrane and electronic phase potentials, respectively. In both Eq. 8 and Eq. 9, first and second term represent through-plane and in-plane charge transport respectively. All the material properties are also considered as anisotropic in order to capture the effect of crack or any gap due to the improper mating of CL/MPL. The source term in the charge equation is used to describe the transfer current between the electronic and electrolyte phase inside of each anode and cathode catalyst layer. In the anode catalyst layer, the kinetic expression represents the hydrogen oxidation reaction (HOR). The HOR kinetic expression is derived by linearizing the Butler-Volmer equation on the assumption that the HOR reaction is facile, and hence the surface over-potential is small. The transfer current density on anode side is expressed as follows:

Anode CL: $$J_{gen} = a{i_{o,a}}^{ref}\left(\frac{C_{H_2}}{C_{H_{2,ref}}}\right)^{1/2}\left(\frac{\alpha_a + \alpha_c}{RT}F\eta\right) \quad [10]$$

In the cathode catalyst layer, the kinetic expression represents the oxygen reduction reaction (ORR). The ORR kinetics are slow, causing high over-potential. This can be represented by Tafel kinetics. The ORR kinetic expression is obtained by neglecting the oxidation branch of the Butler-Volmer equation for the cathode [8]:

Cathode CL: $$J_{gen} = -a{i_{o,c}}^{ref}\left(\frac{C_{O_2}}{C_{O_{2,ref}}}\right)\left(-\frac{\alpha_c}{RT}F\eta\right) \quad [11]$$

For other components, the source term is zero. The over-potential is defined as:

$$\eta = \varphi_s - \varphi_e - U_{oc} \quad [12]$$

where U_{oc} is the open-circuit potential which is zero on anode side. The expression for cathode side can be written as [11]:

$$U_{oc} = 1.23 - 9.0 \times 10^{-4}(T - 298.15) \quad [13]$$

As Nafion solution is used as the ionomer in the anode and cathode catalyst layers, the effective proton conductivity of the anode and the cathode catalyst layers follows that of a Nafion membrane but with the Bruggmann correlation, it is represented as:

$$\kappa^{eff} = {\varepsilon_{mc}}^{1.5}\kappa \quad [14]$$

where ε_{mc} is the volume fraction of ionomer in the CL.

Treatment of Cathode Interfacial Layer

To investigate the effect of the interface between the cathode CL|MPL on PEFC performance, an additional layer consisting of MPL, CL surface and interfacial gaps was added to the computational domain. A schematic is shown in Figure 2. To develop this interfacial layer, surfaces of CL and MPL samples were characterized using optical profilometry to obtain the surface characteristics and profile data for digital reconstruction [13]. An interfacial morphological model was also developed at the Penn State FCDDL to obtain the resulting interface under compression [13, 14]. This digitally reconstructed interface was incorporated in the computational domain as shown in Fig. 2b. This interface layer consists of three parts: CL, MPL and void. Appropriate properties of each component were specified in each grid, depending on which region they were. The void region inside the interface layer is modeled as infinite resistivity for electron and proton transport, gas channel diffusivity of species transport and air thermal conductivity for thermal transport. In a flooded scenario, this void space can be filled by liquid water and can block the transport of reactant gases. Additional effort is underway to account for the liquid water treatment in the model frame work and will be presented in the future.

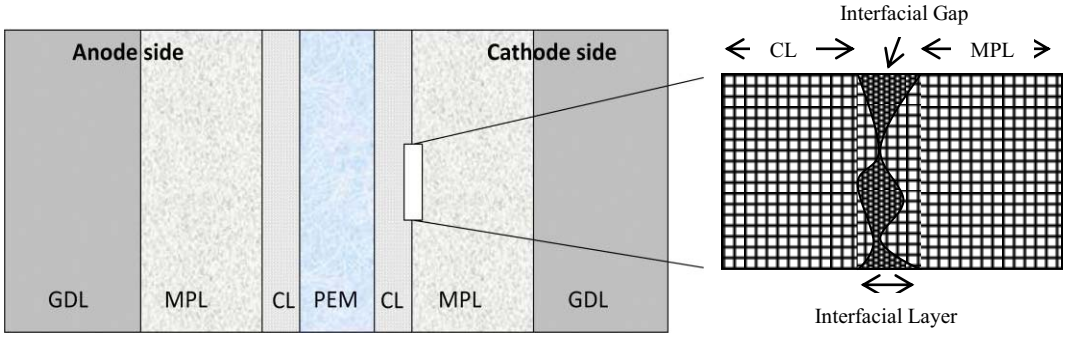

(a) (b)

Figure 2. (a) PEFC Schematic (b) Computational grid and interface layer

Boundary Conditions

The boundary conditions need to be specified in the through plane direction (*x*-direction) only. Boundaries in other direction are symmetric; hence all gradients on these boundaries will be zero. By use of the single domain approach, the boundary conditions are only required at the external surfaces of the computational domain. At the anode/cathode inlet, the inlet species concentrations are determined by the inlet pressure and humidity conditions. For the thermal boundary conditions, a constant temperature is applied to the anode and cathode.

Properties and Parameters

Details of the cell dimension and other modeling parameter are listed in Table I and II. Transport properties and correlations used for Nafion are listed in Table III.

TABLE I. Cell dimension and modeling parameters

Symbol	Parameter	Value [Reference]	Unit
t_{DM}	Anode/Cathode DM thickness	360 [10]	μm
t_{MPL}	Anode/Cathode MPL thickness	40 [10]	μm
t_{CL}	Anode/Cathode CL thickness	10 (Gore Series MEA) [6]	μm
t_m	Membrane thickness	18 (Gore Series MEA) [6]	μm
ε_{DM}	DM porosity	0.6 [15]	-
ε_{MPL}	MPL porosity	0.3	-
ε_{CL}	CL porosity	0.6 [15]	-
ε_{mc}	Volume fraction of ionomer in CL	0.26 [15]	-
$ai_{o,a}$	Exchange current density (anode)	10^9 [15]	A/m^3
$ai_{o,c}$	Exchange current density (cathode)	10^4 [15]	A/m^3
$D_{o,c}$	Diffusion coefficient of oxygen in cathode	3.2348 x 10^{-5}	m^2/s
$D_{o,a}$	Diffusion coefficient of hydrogen in anode	1.1028 x 10^{-4}	m^2/s
$D_{w,c}$	Diffusion coefficient of water vapor in cathode	7.35 x 10^{-5}	m^2/s
F	Faraday constant	96487	C/mol
R	Universal gas constant	8.314	J/molK
$C_{H2,ref}$	Reference hydrogen molar concentration	40	mol/m^3
$C_{O2,ref}$	Reference oxygen molar concentration	40	mol/m^3
α_a	Anodic transfer coefficient for HOR	1 [15]	-
α_c	Cathodic transfer coefficient for HOR	1 [15]	-
α_c	Cathodic transfer coefficient for ORR	1 [15]	-
ΔS_a	Change in entropy for anode	0.104 [18]	J/molK
ΔS_c	Change in entropy for cathode	-326.36 [18]	J/molK

TABLE II. Material properties values for fuel cell components

Symbol	Property	Diffusion Media [Reference]	Micro Porous Layer [Reference]	Catalyst Layer [Reference]	Polymer Electrolyte Membrane [Reference]
σ_x	Through plane electronic conductivity	300 [6]	300 [6]	200 [6]	-
σ_y	In plane electronic conductivity	3000 [6]	300 [6]	200 [6]	-
k_x	Through plane thermal conductivity	0.42 [16]	0.42 [16]	0.27 [16]	0.16 [16]
k_y	In plane thermal conductivity	4.2 [16]	4.2 [16]	2.7 [16]	0.16 [16]

TABLE III. Material properties expressions

Symbol	Property	Expression	Reference
κ	Ionic conductivity	$(0.5139\lambda - 0.326)exp\left[1268\left(\frac{1}{303} - \frac{1}{T}\right)\right]$	[17]
n_d	Drag coefficient	$\frac{2.5\lambda}{22}$	[17]
λ	Water content	$\begin{cases} 0.043 + 17.81a - 39.85a^2 + 36.0a^3, & 0 < a \leq 1 \\ 14 + 1.4(a-1) & for\ 1 < a \leq 3 \end{cases}$	
a	Water acivity	$\frac{C_w RT}{P^{sat}}$	
P^{sat}	Saturation pressure	$log_{10}P = -2.1794 + 0.02953(T - 273.15) - 9.1837 \times 10^{-5}(T - 273.15)^2 + 1.4454 \times 10^{-7}(T - 273.15)^3$	
D_w	Diffusivity of water in membrane	$\begin{cases} 3.1 \times 10^{-7}\lambda\left(e^{0.28\lambda} - 1\right).e^{(-2346/T)}, 0 < \lambda \leq 3 \\ 4.17 \times 10^{-8}\lambda\left(1 + 161e^{-\lambda}\right).e^{(-2346/T)}\ otherwise \end{cases}$	[19]
D_i	Diffusivity of species	$D_o\left(\frac{T}{T_o}\right)^{3/2}\left(\frac{P_o}{P}\right)$	

Results and Discussions

To investigate the effect of interfacial morphology on the PEFC performance, two different cases were simulated. In the first case, interface layer consisting of MPL, CL surface and interfacial gaps was added on the computational domain. The precise morphology of this interface region was obtained from the experimental data for the CL and MPL as discussed before. In the second case, the interfacial region was not accounted for and a perfect contact was assumed. Figure 3 shows comparison of polarization curves for both the cases. It can be seen that there is a decrease in performance due to the addition of interface layer into the computational framework. PEFC losses increases with increase in current density, indicating a potential increase in the ohmic losses. At 1 A/cm^2, voltage drop of 41.7mv is estimated for the case with interface layer. To further investigate the performance loss, the associated impact on charge, energy and mass transport was also studied.

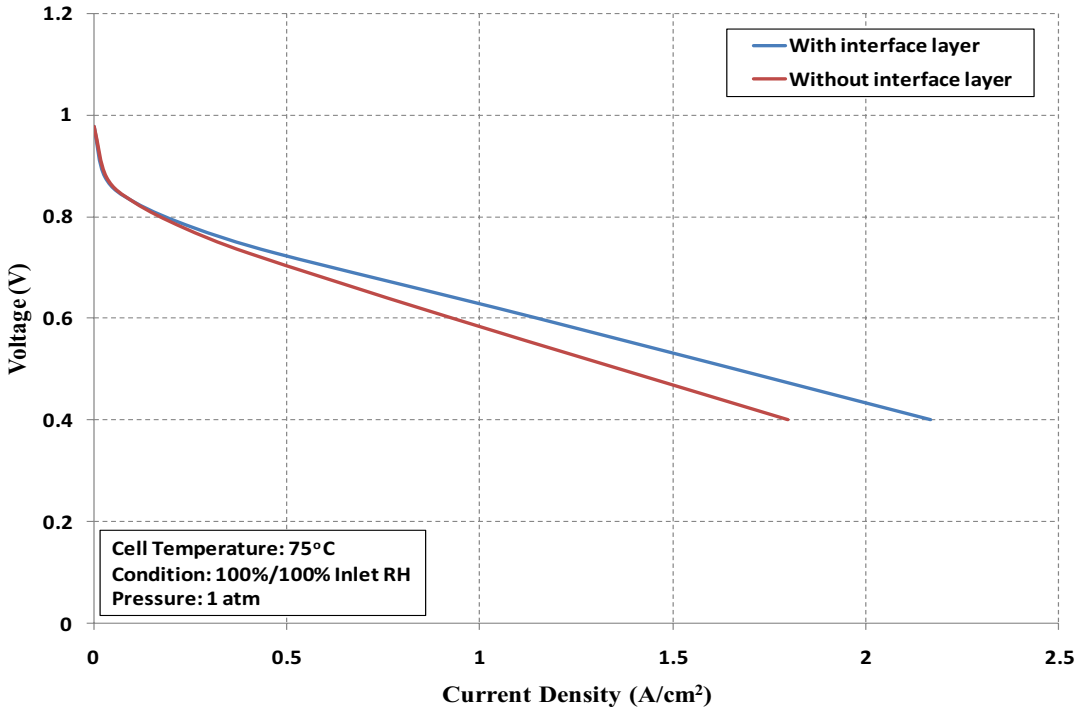

Figure 3. Polarization curve comparison of models with and without interface layer.

Figure 2 shows the impact on charge transport due to the incorporation of the interface layer in the model. Figure 2(a) shows the current distortions caused by the gaps at the CL|MPL interface on cathode side of fuel cell at 1 A/cm^2 current density. Significant in-plane current flow seen in Fig. 2(a) can be caused by the distortion of the voltage contour near the gaps at the interface. The in-plane current flow caused by interfacial gaps seems to increases the ohmic loss of PEFC. Figure 2(b) shows the voltage change of the case with interface layer as compared to the case without interface layer. It can be seen that there is a net decrease in voltage values for the case with interface layer due to the increase in ohmic losses. The maximum change in voltage is found to be 70mv, which is close to the interfacial gaps due to the larger effective mean current flow path.

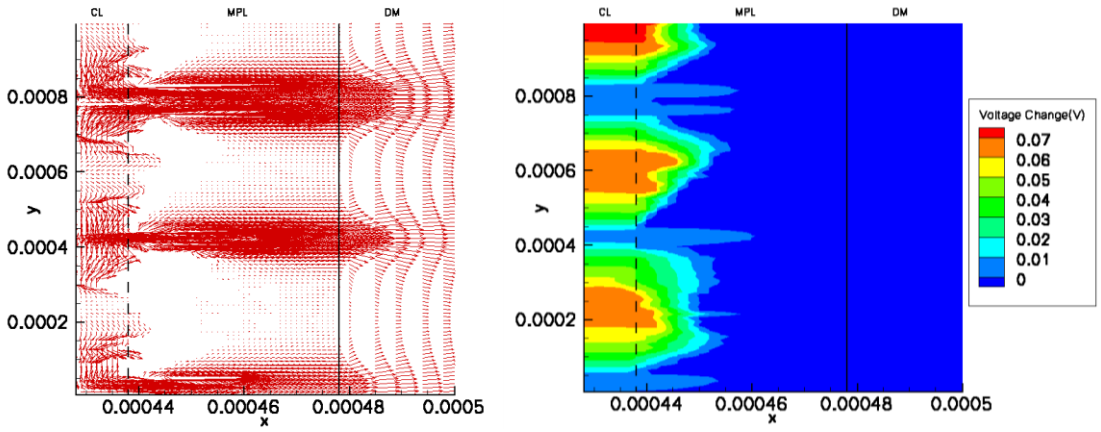

(a) (b)

Figure 2. (a) Vector plot of electron current on cathode side of PEFC. (b) Contour plot of voltage change with and without interface layer.

Figure 3 shows the predicted impact on temperature profile of PEFC with the inclusion of interfacial layer on the cathode side of PEFC. The predictions show a temperature drop for the case with interface layer, as compared to the case without interface layer. The primary reason for temperature drop can be attributed to the absence of heat generation term in the void. This decrease in temperature may also lead to the formation of cold spots in the CL or MPL, and the potential for liquid pooling location.

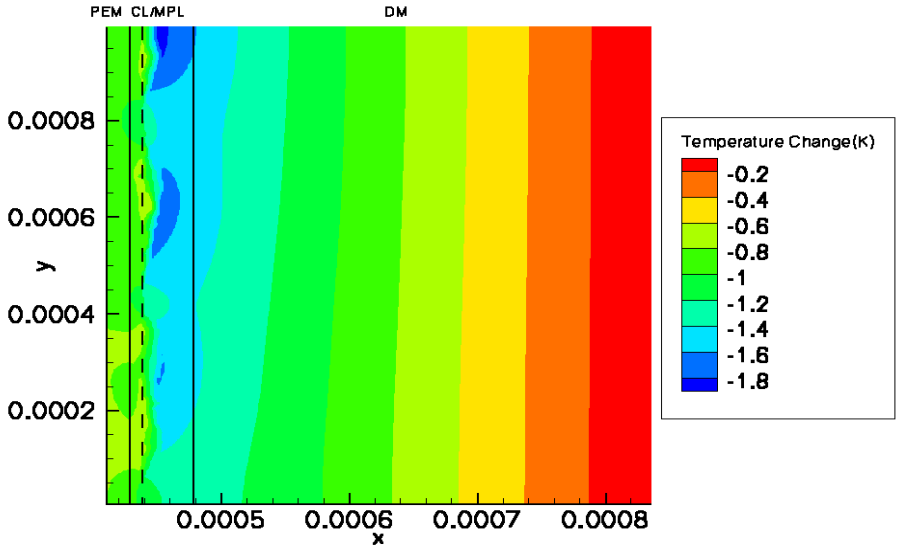

Figure 3. Contour plot of temperature change with and without interface layer.

Figure 4 shows the impact on mass transport with the inclusion of interfacial layer on the cathode side of PEFC. It shows the oxygen mole fraction change in the case with the interface layer, as compared to the case without the interface layer. At these voids, there is no electrochemical reaction, therefore there is no consumption of oxygen. This could be the potential reason for mole fraction increase, observed in these predictions.

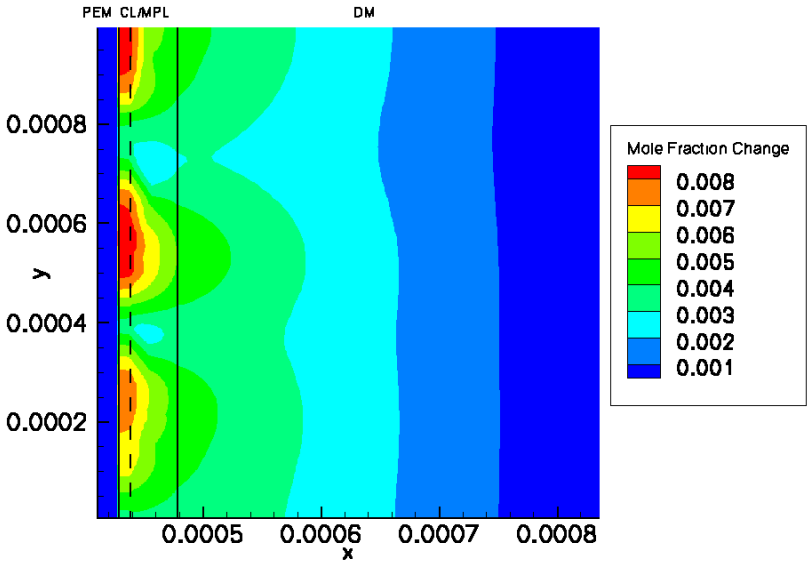

Figure 4. Contour plot of oxygen mole fraction change with and without interface layer.

Summary and Future Work

A single-phase anisotropic mathematical model was developed to investigate the effect of interfacial morphology on fuel cell performance. The novel feature of the model is the inclusion of directly measured surface morphological information of catalyst layer and the micro porous layer. Morphology information shows the existence of cracks and interfacial gaps present in CL|MPL interface. Simulations predicted a decrease in performance of fuel cell for the case with interface layer, which can be attributed to the increase in effective mean current flow path. There is a formation of cold spots near CL|MPL interface in case with interface layer, which can become a pooling location for liquid water. It was also predicted that in case with interface layer, there is an increase in mole fraction of oxygen on cathode side. Further investigations are underway to understand the impact on liquid water transport.

Nomenclature

Symbol	Parameter	Units
MPL	Micro Porous layer	-
CL	Catalyst layer	-
DM	Diffusion media	-
MEA	Membrane electrode assembly	-
C	Concentration	mol/m^3
D	Diffusivity	m^2/s
T	Temperature	K
K	Thermal conductivity	W/mK
φ	Voltage	V
I	Current	A
κ	Ionic conductivity	S/m
σ	Electronic conductivity	S/m
P	Pressure	Pa
F	Faraday constant	C/mol
R	Universal gas constant	J/mol K
λ	Water content	-
A	Water activity	-
α	Transfer coefficient	-
U	Open circuit voltage	V
ε	Porosity	-
ΔS	Change in entropy	J/K
η	Overpotential	V

Subscript	Parameter
X	Through plane direction
Y	In plane direction
E	Ionic
S	Electronic
OC	Open circuit
I	Species index
W	Water
A	Anode
C	Cathode

Acknowledgments

This work was supported by the Toyota Motor Corporation, Japan. M. M. Mench thanks NSF CAREER award # 0644811 for partial support.

References

1. B. Avasarala, P. Haldar, *J. Power Sources*, **188** (1), 225 (2009).
2. I. Nitta, O. Himanen, M. Mikkola, *Electrochemistry Communications*, **10** (1), 51 (2008).
3. R. Makharia, M.F. Mathias and D.R. Baker, *J. Electrochem. Soc.*, **152** (5), A970 (2005).
4. S. Kim, and M. M. Mench, *J. Power Sources*, **174** (1), 206 (2007).
5. S. Kim, B. K. Ahn, and M. M. Mench, *J. Power Sources*, **179** (1), 140 (2008).
6. S. Kim, M. Khandelwal, and M. M. Mench, *J. Electrochem. Soc.*, **156** (1), B99 (2009).
7. M. Khandelwal, H. Bajpai, S. Kim, E. C. Kumbur, and M. M. Mench, Presented in the *First International Forum on Multidisciplinary Education and Research for Energy Science (GCOE conference),* Tokyo, Japan (2008).
8. M. M. Mench, *Fuel Cell Engines*, John Wiley & Sons (2008).
9. S. Kim and M. M. Mench, *J. Membrane Science*, **328** (1), 113 (2009).
10. M. Khandelwal, S. Lee and M. M. Mench, *J. Power Sources*, **172** (1), 816 (2007).
11. D. Poulikakos, *Conduction Heat Transfer*, Englewood Cliff (1994).
12. C. Berger, *Handbook of Fuel Cell Technology*, Englewood Cliffs (1968).
13. F. E. Hizir, T. Swamy, S. O. Ural, E. C. Kumbur and M. M. Mench, *Proceedings of The 7th International Conference on Fuel Cell Science Engineering and Technology*, 85092 (2009), in press.
14. T. Swamy, F. E. Hizir, M. Khandelwal, E. C. Kumbur and M. M. Mench, *Electrochemical Society (ECS) Transactions*, (2009).
15. H. Ju, H. Meng and C Y Wang, *J. Heat and Mass Transfer*, **48** (1), 1303 (2005).
16. M. Khandelwal and M. M. Mench, *J. Power Sources*, **161** (1), 1106 (2006).
17. E. Springer, T. A. Zawodzinski, and S. Gottesfeld, *J. Electrochem. Soc.*, **138** (1), 2334 (1991).
18. M.J. Lampinen, M. Fomino, *J. Electrochem. Soc.,* **140** (12), 3537 (1993).
19. Motupally, A. J. Becker, and J. W. Weidner, *J. Electrochem. Soc.*, **147** (1), 3171 (2000).